

## Supporting information

### **A flame retardant poly vinyl alcohol/graphene oxide/phytic acid composite for quick response and ultra-long fire alarm**

Zhihao Zhang<sup>a,b</sup>; Zhenzhu Zhou<sup>a,b</sup>; Junchao Huang<sup>a,b,\*</sup>; Yuhua Wang<sup>a,b,\*</sup>

<sup>a</sup> School of Materials and Energy, Lanzhou University, Lanzhou, 730000, China

<sup>b</sup> Key Laboratory of Special Function Materials and Structure Design, Ministry of Education, Lanzhou, 730000, China

Corresponding author email: [wyh@lzu.edu.cn](mailto:wyh@lzu.edu.cn)

## Experimental section

### Materials

Poly (vinyl alcohol) ( $1750 \pm 50$ ) (PVA) was supplied in Sinopharm Chemical Reagent (Shanghai, China). Phytic acid ( $M_w \sim 660$ , 50 wt.% *aq.*) was provided by Aladdin Chemistry (Shanghai, China). Concentrated sulfuric acid ( $H_2SO_4$ , ~98 wt.%) and concentrated hydrochloric acid (HCl, 36 ~ 38 wt.%) were bought from Kelong Chemical Co., Ltd (Chengdu, China). Natural graphite, potassium permanganate ( $KMnO_4$ ), sodium nitrate ( $NaNO_3$ ), and hydrogen peroxide solution ( $H_2O_2$ , 30 vol.%) were gained from Pfizer Industry Inc. (Gansu, China). All chemicals were analytical grade and used without further purification.

### Instruments and Measurement

The X-Ray Diffraction (XRD) patterns were measured by Rigaku D/Max-2400 X diffraction with Ni-filtered Cu  $K\alpha$  radiation ( $\lambda = 0.154$  nm) from  $5^\circ$  to  $60^\circ$  with a scanning speed of  $15^\circ \cdot \text{min}^{-1}$ .

The Fourier transform infrared spectra (FTIR) were performed on a Nicolet NEXUS 670 (USA) spectrometer within the scanning range of  $4000 \sim 400$   $\text{cm}^{-1}$ .

Raman spectroscopy (Horiba, France) was carried out to analyze the degree of graphitization of the char residues. The excitation was set to 528 nm to acquire the information in the range of  $2000 \sim 500$   $\text{cm}^{-1}$ .

A PHI-5702 photoelectron spectrometer with an Al  $K\alpha$  excitation source (1.486 keV) was applied to record the X-ray photoelectron spectroscopy (XPS) spectra for the analysis of element composition and chemical structure of all samples.

A scanning electron microscope (SEM) (S-3400, Hitachi, Japan) was utilized to

investigate the micromorphological features of PVA and PGP composite films as well as their residual char layer after combustion. The composition and dispersibility of elements were characterized by energy-dispersive spectrometry (EDS) (X-Max, Oxford Instruments, UK) equipped with SEM.

The fluorescence microscopy (DSX100, Olympus, Japan) was utilized to observe the surface morphology of PVA, P<sub>1</sub>G<sub>1</sub> nanocomposites and P<sub>1</sub>G<sub>1</sub>P<sub>0.8</sub> nanocomposites by the bright and dark field, and the green light mode with a wavelength range of 460 ~ 550 nm.

The 3D measurement laser microscope (OLS5000, Olympus, Japan) is used to observe and measure the surface roughness of the PGP nanocomposites.

Thermogravimetric analysis (STA PT 1600, Linseis, Germany) was used to analyze the thermal stability at a heating rate of 15 °C·min<sup>-1</sup> from room temperature to 800 °C in N<sub>2</sub>.

A Microscale Combustion Calorimeter (MCC) from Fire Test Technology Limited of the UK was used to analyze fire retardant performance. The weight of all samples was 4.5 ~ 5 mg. All samples were heated from 150 to 600 °C at a heating rate of 1 °C/s.

The universal testing machine (CMT 8502, Instron, USA) was used to measure the tensile strength of PVA and PGP composite films. The samples were cut into dumbbell shapes with a width and length of 5 mm and 40 mm according to GB/T 1040.3-2006 standard. The tensile speed was set as 50 mm/min. Young's modulus  $E$  was calculated from the initial linear region of the tensile stress-strain curves. Herein,  $\sigma_b$  and  $\varepsilon_b$  referred to the tensile stress and the strain at break, respectively. The work of fracture ( $W_f$ ) was calculated according to the mathematic area of the tensile stress-strain curve to demonstrate the toughness of the PVA and PGP composite films.

In the fire warning test, the fire alarm system, composed of a PGP

nanocomposites strip, LED lamp, power source and some wires, is built according the circuit diagram of the Fig. 5a. For the burning situation, the samples were exposed directly to ethanol flame for some time and then the warning trigger and duration time was recorded. For the low temperature heating situation, a hot plate (JF-956A, Jftoois, China) was employed to exert the different temperatures (100, 150, 200, 250, 300, and 350 °C) on the PGP nanocomposite films or the cotton fabric coated with  $P_1G_1P_{0.8}$ . Then the samples were taken down to determine whether they can light up the LED lamp at an appropriate time and the time was recorded. Meanwhile, the electrical resistance changing curve of the samples during heating or burning was recorded with a digit multimeter (VC990C+, Victor Instrument, China).

## Supplementary Figures and Tables

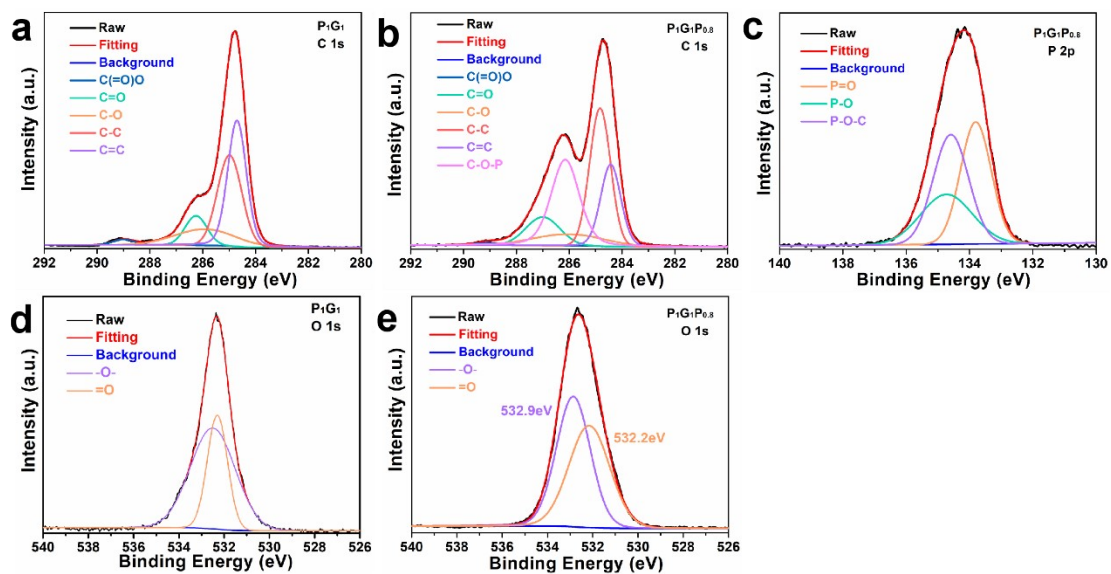


**Fig. S1** The high-resolution XPS spectra of C1s of  $P_1G_1$  (a), C1s of  $P_1G_1P_{0.8}$  (b), P2p of  $P_1G_1P_{0.8}$  (c), O1s of  $P_1G_1$  (d) and O1s of  $P_1G_1P_{0.8}$  (e).

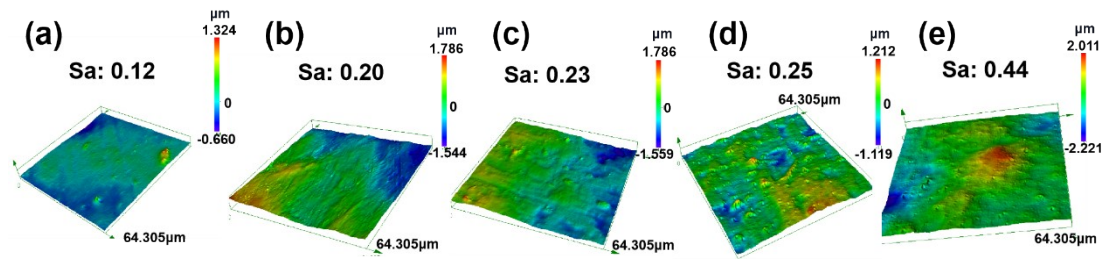


**Fig. S2** The surface roughness (Sa) of  $P_1G_1$  (a),  $P_1G_1P_{0.2}$  (b),  $P_1G_1P_{0.4}$  (c),  $P_1G_1P_{0.6}$  (d), and  $P_1G_1P_{0.8}$  (e) nanocomposites.

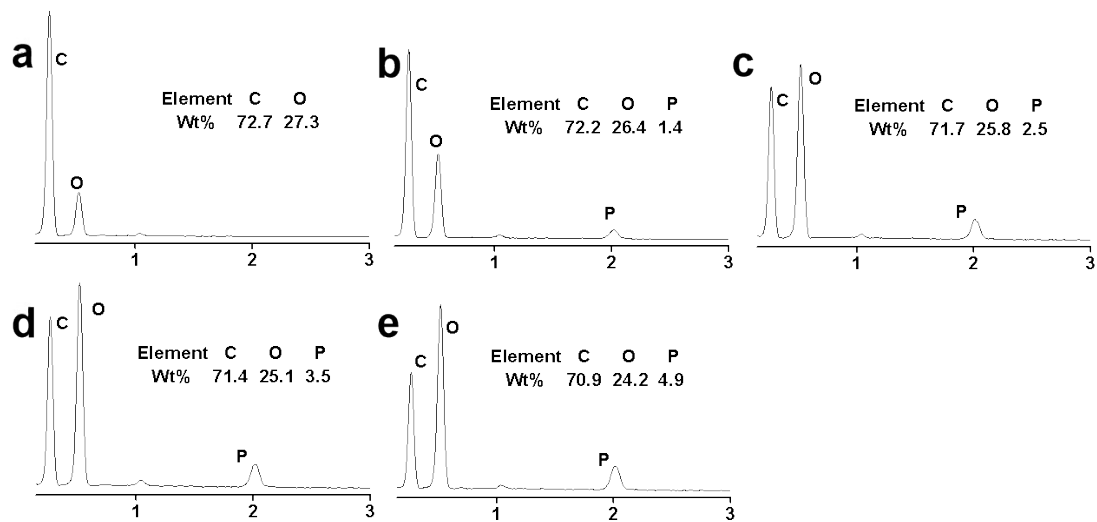


**Fig. S3** The EDS spectra and element contents of  $P_1G_1$  (a),  $P_1G_1P_{0.2}$  (b),  $P_1G_1P_{0.4}$  (c),  $P_1G_1P_{0.6}$  (d), and  $P_1G_1P_{0.8}$  (e) nanocomposites.

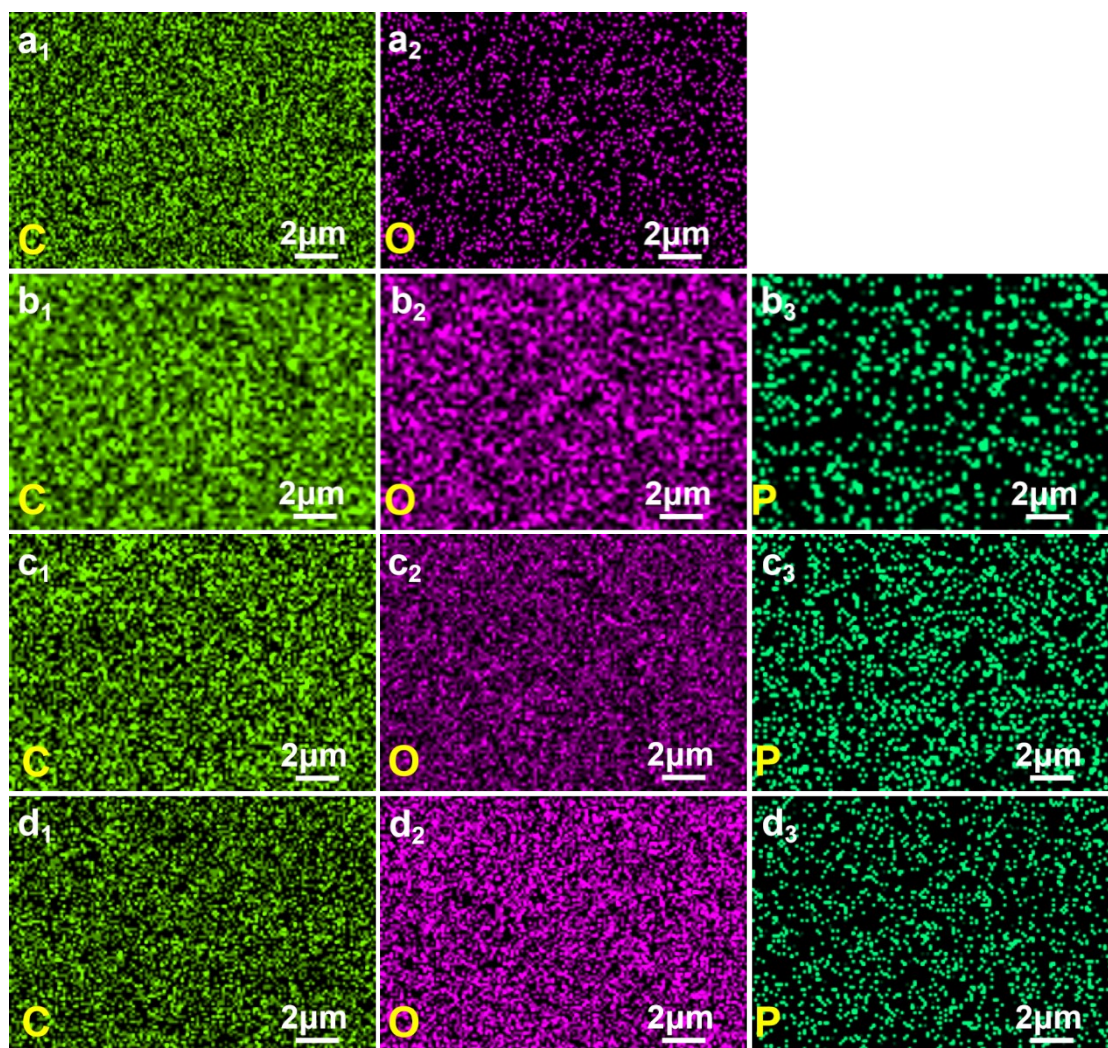


**Fig. S4** The images of EDS mapping for: (a<sub>1</sub>, a<sub>2</sub>) P<sub>1</sub>G<sub>1</sub>, (b<sub>1</sub>-b<sub>3</sub>) P<sub>1</sub>G<sub>1</sub>P<sub>0.2</sub>, (c<sub>1</sub>-c<sub>3</sub>) P<sub>1</sub>G<sub>1</sub>P<sub>0.4</sub>, and (d<sub>1</sub>-d<sub>3</sub>) P<sub>1</sub>G<sub>1</sub>P<sub>0.6</sub> nanocomposites.

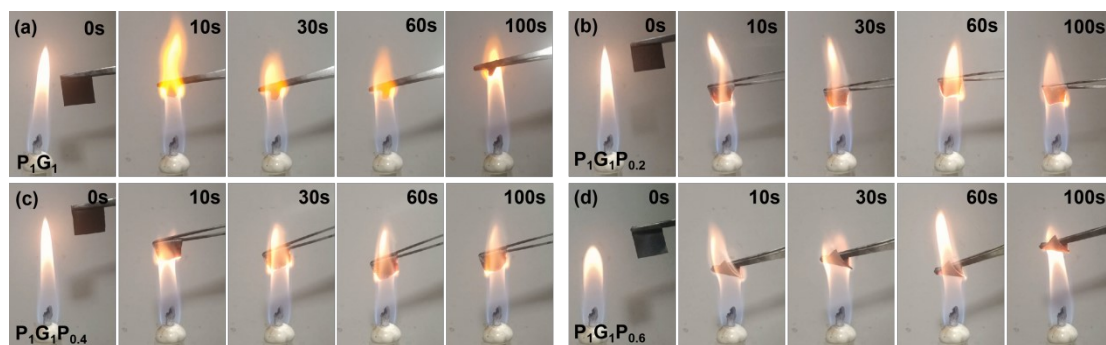


**Fig. S5** The snapshots of  $P_1G_1$  (a),  $P_1G_1P_{0.2}$  (b),  $P_1G_1P_{0.4}$  (c) and  $P_1G_1P_{0.6}$  (d) nanocomposites during combustion process.

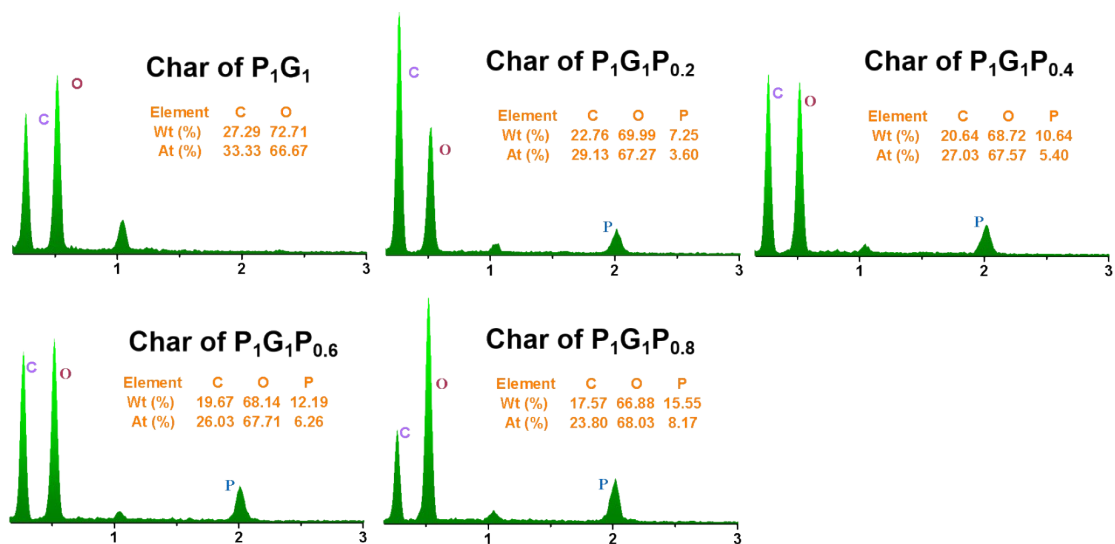


**Fig. S6** EDS spectra and element content of char residues of each PGP sample.

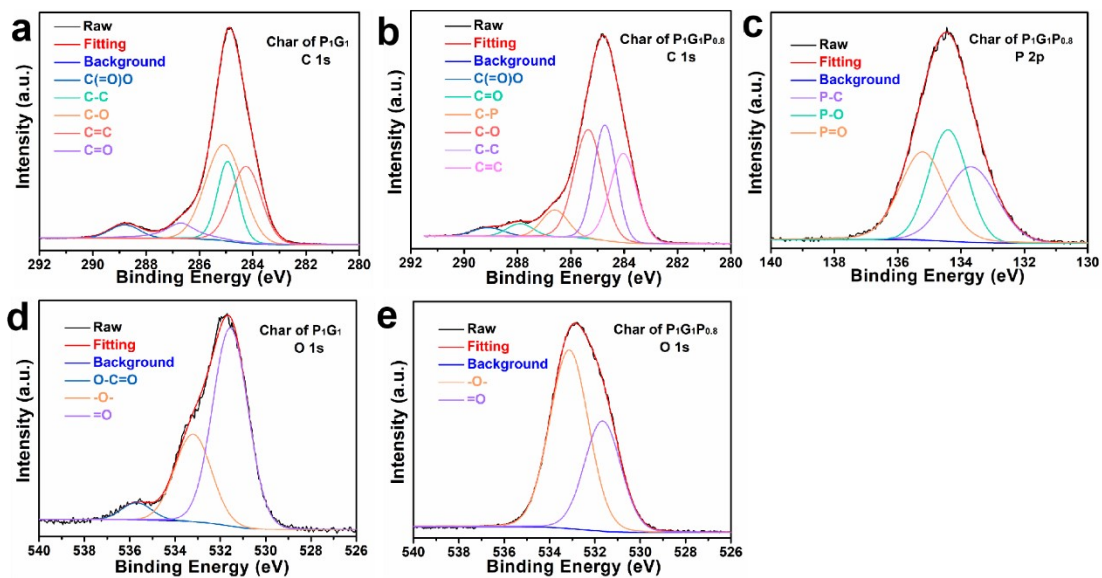


**Fig. S7** The high-resolution XPS spectra for the char residue of  $P_1G_1$  and  $P_1G_1P_{0.8}$  nanocomposites.

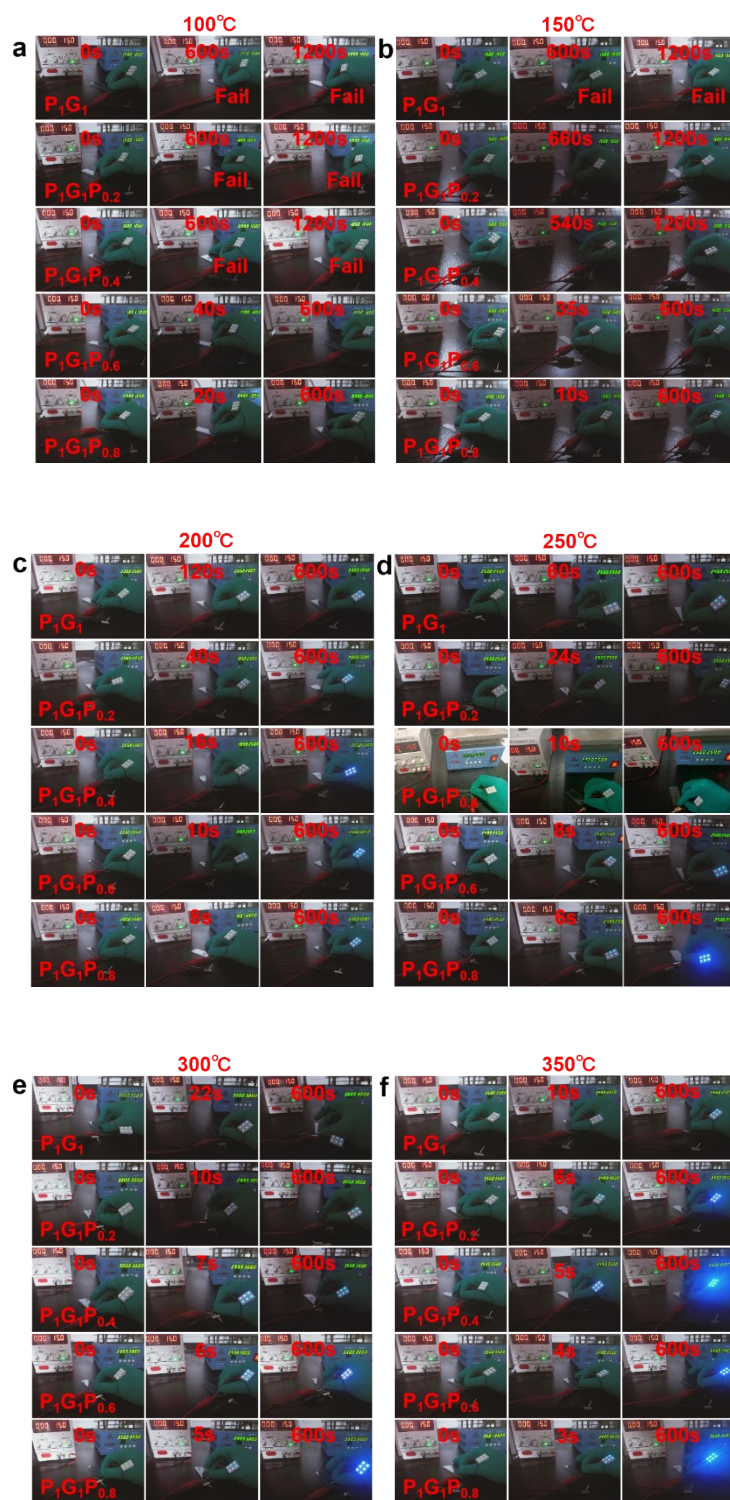


**Fig. S8** The snapshots of the fire warning process of PG and PGP nanocomposites at a relatively low temperature: (a) 100 °C, (b) 150 °C, (c) 200 °C, (d) 250 °C, (e) 300 °C, and (f) 350 °C.



**Fig. S9** The fire warning process snapshots of different-sized  $P_1G_1P_{0.8}$  nanocomposite film under fire attack.

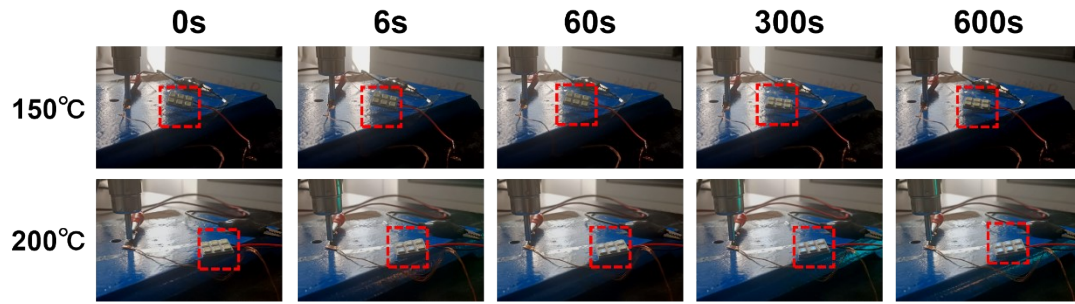


**Fig. S10** The warning process of  $P_1G_1P_{0.8}$  nanocomposites (size:  $0.8 \times 4 \text{ cm}^2$ ) under 150 and 200 °C concentrated air heating using a nozzle with a diameter of 0.5 cm.

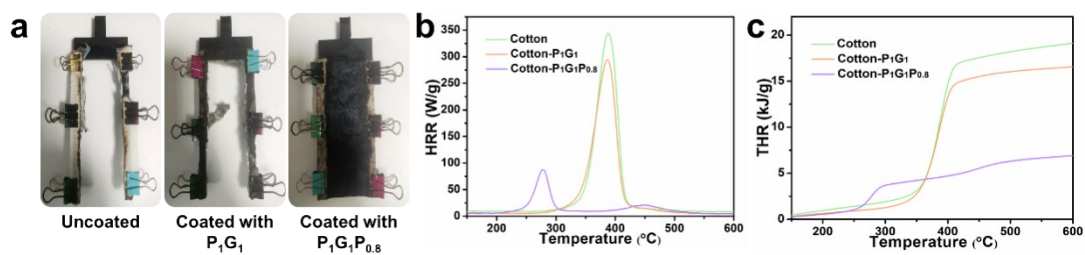


**Fig. S11** (a) The images of char layers of pure cotton, cotton coated with P<sub>1</sub>G<sub>1</sub>, and cotton coated with P<sub>1</sub>G<sub>1</sub>P<sub>0.8</sub> after the combustion test. The HRR (b) and THR (c) curves of pure cotton, cotton coated with P<sub>1</sub>G<sub>1</sub>, and cotton coated with P<sub>1</sub>G<sub>1</sub>P<sub>0.8</sub>.

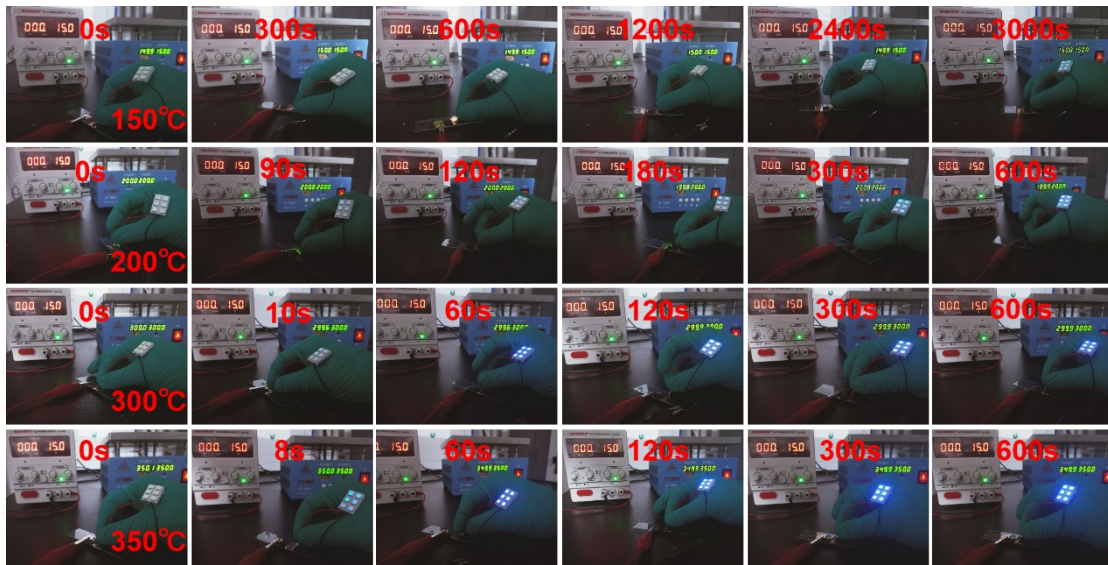


**Fig. S12** The fire warning process of cotton fabric coated with  $P_1G_1P_{0.8}$  under different temperatures.

**Table S1.** The fitted chemical bond modes and their binding energy and percentage in the high-resolution C1s and P2p spectra of P<sub>1</sub>G<sub>1</sub> and P<sub>1</sub>G<sub>1</sub>P<sub>0.8</sub> before and after combustion.

Sample/ Spectral line	Before combustion			After combustion		
	Chemical bonds	Binding energy (eV)	Percentage (%)	Chemical bonds	Binding energy(eV)	Percentage (%)
P <sub>1</sub> G <sub>1</sub> C1s	C(=O)-O	289.0	1.72	C(=O)-O	288.8	4.49
	C=O	286.3	9.93	C=O	286.7	7.79
	C-O	285.9	15.01	C-O	285.1	40.50
	C-C	285.0	34.17	C-C	284.9	20.05
	C=C	284.7	39.17	C=C	284.2	27.17
P <sub>1</sub> G <sub>1</sub> P <sub>0.8</sub> C1s	C(=O)-O	289.1	0.62	C(=O)-O	289.1	2.71
	C=O	287.0	10.45	C=O	287.9	3.44
	C-O	286.2	29.86	C-O	285.3	33.20
	C-C	284.8	31.44	C-C	284.7	27.72
	C=C	284.4	18.82	C=C	284.0	25.60
	C-O-P	286.0	8.81	C-P	286.6	7.33
P <sub>1</sub> G <sub>1</sub> P <sub>0.8</sub> P2p	P=O	133.8	36.76	P=O	135.2	34.33
	P-O	134.8	25.26	P-O	134.4	34.38
	P-O-C	134.5	37.98	P-C	133.7	31.29

**Table S2.** Summary of the mechanical strength of PVA and PGP composite films.

<b>Sample</b>	<b><math>\sigma_b</math> (MPa)</b>	<b><math>\varepsilon_b</math> (%)</b>	<b><math>E</math> (GPa)</b>	<b><math>W_f</math> (MJ·m<sup>-3</sup>)</b>
PVA	60 ± 1	217 ± 5	1.5 ± 0.08	115 ± 5
P <sub>1</sub> G <sub>1</sub>	121 ± 3	8 ± 1	2.2 ± 0.10	10 ± 2
P <sub>1</sub> G <sub>1</sub> P <sub>0.2</sub>	79 ± 2	28 ± 4	1.8 ± 0.14	21 ± 2
P <sub>1</sub> G <sub>1</sub> P <sub>0.4</sub>	68 ± 2	75 ± 2	0.8 ± 0.07	43 ± 4
P <sub>1</sub> G <sub>1</sub> P <sub>0.6</sub>	64 ± 1	247 ± 3	0.5 ± 0.06	136 ± 3
P <sub>1</sub> G <sub>1</sub> P <sub>0.8</sub>	55 ± 3	357 ± 9	0.2 ± 0.05	167 ± 4

**Table S3.** The mechanical comparison with reported PVA composite films regarding their toughness and modulus.

<b>PVA composite films</b>	<b><i>E</i> (GPa)</b>	<b><i>W<sub>f</sub></i> (MJ·m<sup>-3</sup>)</b>	<b><i>Dosage</i> (wt%)</b>	<b><i>Reference</i></b>
GO/PVA-1	5.8	0.9	95.0	[1]
RGO/PVA	10.4	2.5	80.0	[1]
GO/PVA-2	36.4	0.1	60.0	[2]
TiO <sub>2</sub> -GO-MMT/PVA	5.2	1.9	50.0	[3]
Al <sub>2</sub> O <sub>3</sub> -GO/PVA	9.0	9.2	39.0	[4]
AOPA/PVA	0.4	80.2	30.0	[5]
sucrose-g-BNNS/PVA	1.7	8.4	20.0	[6]
Nanoclay/PVA	0.2	95.9	10.0	[7]
TE/PVA	4.2	250.8	5.0	[8]
BP-sucrose(N)/PVA	1.2	46.1	0.5	[9]
OH-BN/PVA	0.4	133.4	0.2	[10]
DGNS/PVA	1.5	4.5	0.1	[11]
PA-GO/PVA	0.2	167.1	64.8	This work

**Table S4.** TG data of PVA and its composites under N<sub>2</sub> atmosphere.

Sample	$T_{\text{dep}}$ (°C) <sup>a</sup>	$T_{\text{max}}$ (°C) <sup>b</sup>	$T_{50\%}$ (°C) <sup>c</sup>	$R_{\text{dpm}}$ (%·°C <sup>-1</sup> ) <sup>d</sup>	Char residues (wt.%)
PVA	230	270	281	1.13	8
P <sub>1</sub> G <sub>1</sub>	245	333	330	0.63	9
P <sub>1</sub> G <sub>1</sub> P <sub>0.2</sub>	195	223	436	0.62	34
P <sub>1</sub> G <sub>1</sub> P <sub>0.4</sub>	164	193	438	0.59	35
P <sub>1</sub> G <sub>1</sub> P <sub>0.6</sub>	163	185	458	0.57	37
P <sub>1</sub> G <sub>1</sub> P <sub>0.8</sub>	162	180	525	0.52	38

<sup>a</sup> The temperature started to decompose.

<sup>b</sup> The temperature reached the maximum decomposition rate.

<sup>c</sup> The temperature reached a weight loss of 50%.

<sup>d</sup> The maximum weight loss rate at  $T_{\text{max}}$ .

**Table S5.** Summary of MCC data of PVA and PGP composites.

Sample	$T_p$ (°C) <sup>a</sup>	pHRR (W·g <sup>-1</sup> )	HRC [J·(g·K) <sup>-1</sup> ]	THR (kJ·g <sup>-1</sup> )
PVA	275	529.9 ± 1.8	508.3 ± 6.9	23.0 ± 0.2
P <sub>1</sub> G <sub>1</sub>	364	159.6 ± 1.2	141.8 ± 4.8	23.9 ± 0.2
P <sub>1</sub> G <sub>1</sub> P <sub>0.2</sub>	460	122.5 ± 1.7	108.9 ± 5.7	12.6 ± 0.3
P <sub>1</sub> G <sub>1</sub> P <sub>0.4</sub>	454	97.8 ± 0.8	89.1 ± 3.8	10.8 ± 0.1
P <sub>1</sub> G <sub>1</sub> P <sub>0.6</sub>	450	76.7 ± 1.5	67.5 ± 4.1	10.0 ± 0.1
P <sub>1</sub> G <sub>1</sub> P <sub>0.8</sub>	445	60.4 ± 0.9	51.3 ± 5.6	7.7 ± 0.1

<sup>a</sup> The temperature reached peak heat release rate (pHRR).

**Table S6.** The electrical resistivity of PG and PGP nanocomposites in different combustion times.

Sample	Electrical resistivity ( $\Omega \cdot \text{m}$ )						
	0	2	4	6	8	10	12
$\text{P}_1\text{G}_1$	$2.4 \times 10^9$	N/A <sup>a</sup>	N/A	N/A	N/A	N/A	N/A
$\text{P}_1\text{G}_1\text{P}_{0.2}$	$8.6 \times 10^5$	$4.5 \times 10^4$	$5.5 \times 10^3$	$2.1 \times 10^3$	$1.4 \times 10^3$	$7.9 \times 10^2$	$7.9 \times 10^2$
$\text{P}_1\text{G}_1\text{P}_{0.4}$	$3.7 \times 10^5$	$3.1 \times 10^4$	$4.8 \times 10^3$	$1.5 \times 10^3$	$1.2 \times 10^3$	$7.9 \times 10^2$	$7.9 \times 10^2$
$\text{P}_1\text{G}_1\text{P}_{0.6}$	$8.3 \times 10^4$	$2.2 \times 10^4$	$3.1 \times 10^3$	$1.2 \times 10^3$	$9.4 \times 10^2$	$7.9 \times 10^2$	$7.9 \times 10^2$
$\text{P}_1\text{G}_1\text{P}_{0.8}$	$6.9 \times 10^4$	$1.3 \times 10^4$	$1.9 \times 10^3$	$1.1 \times 10^3$	$7.9 \times 10^2$	$7.9 \times 10^2$	$7.9 \times 10^2$

<sup>a</sup> The sample was burned to highly disintegrate and was unable to measure the resistivity.

**Table S7.** The response time of different samples at different temperatures.

Sample	Response time (s)					
	100°C	150°C	200°C	250°C	300°C	350°C
P <sub>1</sub> G <sub>1</sub>	Fail <sup>a</sup>	Fail	120	60	22	10
P <sub>1</sub> G <sub>1</sub> P <sub>0.2</sub>	Fail	660	40	24	10	6
P <sub>1</sub> G <sub>1</sub> P <sub>0.4</sub>	Fail	540	16	10	7	5
P <sub>1</sub> G <sub>1</sub> P <sub>0.6</sub>	40	35	10	8	6	5
P <sub>1</sub> G <sub>1</sub> P <sub>0.8</sub>	20	10	8	6	5	4

<sup>a</sup> No electric response.

**Table S8.** MCC data of cotton and coated cotton.

Sample	pHRR ( $\text{W}\cdot\text{g}^{-1}$ )	$T_p$ ( $^{\circ}\text{C}$ )	HRC [ $\text{J}\cdot(\text{g}\cdot\text{K})^{-1}$ ]	THR ( $\text{kJ}\cdot\text{g}^{-1}$ )	Char residues (wt.%)
Cotton	$345.6 \pm 3.8$	388	$334.8 \pm 2.9$	$19.2 \pm 0.2$	3
Cotton- $\text{P}_1\text{G}_1$	$296.1 \pm 3.2$	387	$288.7 \pm 4.7$	$16.6 \pm 0.2$	5
Cotton- $\text{P}_1\text{G}_1\text{P}_{0.8}$	$87.7 \pm 4.9$	278	$81.4 \pm 3.6$	$6.9 \pm 0.1$	33

## Reference

- [1] Y.Q. Li, T. Yu, T.Y. Yang, L.X. Zheng, K. Liao, Bio-inspired nacre-like composite films based on graphene with superior mechanical, electrical, and biocompatible properties, *Advanced Materials* 24 (2012) 3426-3431.
- [2] K.W. Putz, O.C. Compton, M.J. Palmeri, S.T. Nguyen, L.C. Brinson, High-Nanofiller-Content Graphene Oxide-Polymer Nanocomposites via Vacuum-Assisted Self-Assembly, *Advanced Functional Materials* 20 (2010) 3322-3329.
- [3] J. Zhang, L. Zhang, C. Li, Modified TiO<sub>2</sub>@graphene oxide and montmorillonite synergistically enhanced multifunctional nanocomposite films, *Polymer Composites* 42 (2021) 2511-2522.
- [4] J. Wang, J. Qiao, J. Wang, Y. Zhu, L. Jiang, Bioinspired Hierarchical Alumina-Graphene Oxide-Poly(vinyl alcohol) Artificial Nacre with Optimized Strength and Toughness, *ACS Applied Materials & Interfaces* 7 (2015) 9281-9286.
- [5] S. Peng, M. Zhou, F. Liu, C. Zhang, X. Liu, J. Liu, L. Zou, J. Chen, Flame-retardant polyvinyl alcohol membrane with high transparency based on a reactive phosphorus-containing compound, *Royal Society Open Science* 4 (2017) 170512.
- [6] S. Chen, R. Xu, J. Liu, X. Zou, L. Qiu, F. Kang, B. Liu, H.M. Cheng, Simultaneous Production and Functionalization of Boron Nitride Nanosheets by Sugar-Assisted Mechanochemical Exfoliation, *Advanced Materials* 31 (2019) e1804810.
- [7] N. Abu-Thabit, A.S. Hakeem, K. Mezghani, E. Ratemi, M. Elzagheid, Y. Umar, A. Primartomo, S. Al Batty, A.K. Azad, S. Al Anazi, A. Ahmad, Preparation of pH-Indicative and Flame-Retardant Nanocomposite Films for Smart Packaging Applications, *Sensors (Basel)* 20 (2020).
- [8] W. Xie, Q. Bao, Y. Liu, H. Wen, Q. Wang, Hydrogen Bond Association to Prepare Flame Retardant Polyvinyl Alcohol Film with High Performance, *ACS Applied Materials & Interfaces* 13 (2021) 5508-5517.
- [9] J. Guo, L. Yang, L. Zhang, C. Li, Simultaneous exfoliation and functionalization of black phosphorus by sucrose-assisted ball milling with NMP intercalating and preparation of flame retardant polyvinyl alcohol film, *Polymer* 255 (2022) 125036.

[10] W. Cai, D. Zhang, B. Wang, Y. Shi, Y. Pan, J. Wang, W. Hu, Y. Hu, Scalable one-step synthesis of hydroxylated boron nitride nanosheets for obtaining multifunctional polyvinyl alcohol nanocomposite films: Multi-azimuth properties improvement, *Composites Science and Technology* 168 (2018) 74-80.

[11] M. Qiu, D. Wang, L. Zhang, M. Li, M. Liu, S. Fu, Electrochemical exfoliation of water-dispersible graphene from graphite towards reinforcing the mechanical and flame-retardant properties of poly (vinyl alcohol) composites, *Materials Chemistry and Physics* 254 (2020) 123430.